Magnetic Resonance in Medicine 42:1137–1145 (1999)

Distribution and Dynamics of Laser-Polarized ^{129}Xe Magnetization In Vivo

Scott D. Swanson,[1]* Matthew S. Rosen,[2] Kevin P. Coulter,[2] Robert C. Welsh,[2] and Timothy E. Chupp[2]

The first magnetic resonance imaging studies of laser-polarized ^{129}Xe, dissolved in the blood and tissue of the lungs and the heart of Sprague-Dawley rats, are described. ^{129}Xe resonances at 0, 192, 199, and 210 ppm were observed and assigned to xenon in gas, fat, tissue, and blood, respectively. One-dimensional chemical-shift imaging (CSI) reveals xenon magnetization in the brain, kidney, and lungs. Coronal and axial two-dimensional CSI show ^{129}Xe dissolved in blood and tissue in the thorax. Images of the blood resonance show xenon in the lungs and the heart ventricle. Images of the tissue resonance reveal xenon in lung parenchyma and myocardium. The ^{129}Xe spectrum from a voxel located in the heart ventricle shows a single blood resonance. Time-resolved spectroscopy shows that the dynamics of the blood resonance match the dynamics of the gas resonance and demonstrates efficient diffusion of xenon gas to the lung parenchyma and then to pulmonary blood. These observations demonstrate the utility of laser-polarized ^{129}Xe to detect exchange across the gas-blood barrier in the lungs and perfusion into myocardial tissue. Applications to measurement of lung function, kidney perfusion, myocardial perfusion, and regional cerebral blood flow are discussed. Magn Reson Med 42:1137–1145, 1999. © **1999 Wiley-Liss, Inc.**

Key words: tissue perfusion; xenon; laser-polarized; hyperpolarized; lung function

The biological properties of xenon and the ability to create high levels of nuclear polarization in noble gases combine to make magnetic resonance imaging (MRI) of laser-polarized ^{129}Xe an exciting field of research. Freely diffusible across biological membranes and metabolically inert, xenon dissolves in blood (1), travels to distant organs, and accumulates in tissue. By applying the principles of diffusible indicators first outlined by Kety (2), radioactive ^{133}Xe has been used in nuclear medicine to measure kidney perfusion (3), cardiac perfusion (4), regional cerebral blood flow (rCBF) (5), and lung ventilation (6). These measurements are possible because the tissue distribution (7) and dynamics of ^{133}Xe in vivo are well understood. To make similar perfusion measurements using MRI of laser-polarized ^{129}Xe, the distribution and dynamics of xenon magnetization in vivo must first be determined.

The most exciting medical applications for laser-polarized (also called hyperpolarized) ^{129}Xe nuclear magnetic resonance (NMR) lie in imaging xenon dissolved in tissue or blood. Previous spectroscopy studies of ^{129}Xe in vivo in the mouse body (8), rat body (9), rat brain (10,11), and human brain and chest (12) demonstrated that xenon in blood, tissue, and gas resonates at different frequencies and suggest that the different frequency components can be selectively imaged. In vitro studies of xenon dissolved in blood have revealed two components, plasma and red blood cell, exchanging rapidly with respect to T_1 but slowly with respect to the inverse frequency separation (13,14). Additional in vitro work has measured the T_1 of xenon dissolved in tissue samples (15). Our initial work focused on imaging ^{129}Xe in the rat brain after inhalation and resulted in the first, chemical-shift resolved image of laser-polarized ^{129}Xe dissolved in tissue (10). No information has been published to date concerning the spatial distribution of xenon magnetization in the whole body in vivo.

The tissue distribution of ^{129}Xe magnetization in vivo will be much different than the distribution of xenon (7) because xenon polarization decays once injected or inhaled. The value of the decay rate differs in the lungs, blood, tissue, and fat. Measuring the xenon magnetization distribution is needed to determine which organs will be suitable for perfusion measurement with laser-polarized ^{129}Xe. Understanding the dynamics of ^{129}Xe magnetization in vivo is essential to new imaging methods that measure tissue perfusion with MRI of laser-polarized ^{129}Xe. This paper presents the first chemical-shift resolved images of ^{129}Xe in blood, tissue, and gas in the thorax, assignments for the in vivo blood and tissue resonances, and a study of the dynamics of laser-polarized ^{129}Xe in vivo. We also discuss how MRI of laser-polarized ^{129}Xe may be used in the future to measure rCBF, cardiac perfusion, kidney perfusion, and lung function.

MATERIALS AND METHODS

Xenon Polarization and Delivery

Xenon was polarized and delivered to Sprague-Dawley rats (200–250 g) by an apparatus previously described (10) and recently modified (11). The current device makes multiple, 165-ml batches of laser-polarized, naturally-abundant xenon (^{129}Xe 26.44%) at a rate of approximately one batch per 5 minutes. ^{129}Xe polarization is typically 5%. Each batch was frozen and stored as xenon ice ($T_1 \cong 1$ hour at 50 mT and 77 K). Between two and five batches of polarized ^{129}Xe were used for each experiment presented here. After freezing of multiple batches, polarized xenon ice was warmed, and the gas expanded into a one-liter glass cylinder sealed by a Teflon piston. A series of automated valves regulated delivery of a 50/50 xenon/oxygen mixture to the animal. Mixing with oxygen occurred just before

[1]Department of Radiology, The University of Michigan, Ann Arbor, Michigan.
[2]Department of Physics, The University of Michigan, Ann Arbor, Michigan.
Grant sponsor: National Institutes of Health; Grant number: GM-48633; Grant sponsor: National Science Foundation; Grant number: PHY-9514340.
*Correspondence to: Scott D. Swanson, Ph.D., Department of Radiology, The University of Michigan, Ann Arbor, MI 48109-0553. E-mail: sswanson@umich.edu
Received 24 November 1998; revised 9 August 1999; accepted 10 August 1999.

inhalation, thereby reducing destruction of xenon magnetization by paramagnetic oxygen (16). Animals were ventilated on the xenon/oxygen mixture for up to 4 minutes at 80 breaths per minute.

Animal and Imaging Procedures

All animal procedures were performed under a protocol approved by the University Committee on the Use and Care of Animals (UCUCA). Three male Sprague-Dawley rats (200–250 g) were used for these studies. Each rat was initially anesthetized with an intraperitoneal injection of ketamine/xylazine mixture (43 mg/kg ketamine, 6 mg/kg xylazine). A 16-gauge, 2.5-inch endotracheal tube was placed and anchored with suture. The animals were ventilated with 2.4 ml per breath of oxygen with a small animal ventilator (Harvard Apparatus, South Natick, MA) at 80 breaths per minute. Anesthesia was maintained with halothane (0.5–1.5%) using a calibrated vaporizer (Fluotec, Buffalo, NY). Pulse rate and oxygen saturation were continuously monitored with a pulse oximeter (Nonin, Plymouth, MN) via a photo transducer pair placed on the tail. Body temperature was maintained at 37°C by a warm water blanket beneath the animal. The rat was placed supine on the experimental platform in a doubly-tuned ^{1}H-^{129}Xe volume probe. The entire assembly of animal, probe, and delivery valve was placed into the magnet during NMR study. Xenon was polarized, stored, and delivered to the animal as previously described (10). Oxygen saturation typically started between 92% and 95%, dropped to 88% during the first minute of xenon/oxygen inhalation, and then returned to 92% for the remaining 3 minutes. Heart rate remained relatively constant throughout xenon/oxygen inhalation. After ^{129}Xe inhalation and study, the animal was switched back to breathing O_2, and the probe was switched for proton imaging. After a number of ^{129}Xe experiments, the animal was euthanized with an overdose of pentobarbital.

NMR Methods

All experiments were performed on a 2.0 T Omega CSI manufactured by General Electric (Fremont, CA) and equipped with self-shielded gradients. A doubly-tuned, slotted-cylinder NMR probe was constructed to resonate at the ^{129}Xe and ^{1}H frequencies, enabling registration of xenon chemical-shift imaging (CSI) data with proton images (17). The probe is 14.5 cm long and 6.0 cm in diameter. To estimate the NMR tip angle, α, the transverse ^{129}Xe magnetization was measured in a closed glass vessel as a function of the number, n, of RF pulses. The decay of transverse magnetization was fitted by the function $M_x(n,\alpha) = \sin(\alpha)\cos^{n-1}(\alpha)M_0$.

Spectroscopy

Spectra of laser-polarized ^{129}Xe in the rat body are shown in Fig. 1. Data collection began before introduction of laser-polarized ^{129}Xe (see Fig. 7) and continued throughout the approximately 40-second xenon inhalation. The full spectrum in Fig. 1 is the sum of three datasets, obtained from one animal, each with 40 seconds of xenon/oxygen breathing. The tip angle was 13°, the pulse width 10 μs, the spectral width 10 kHz, and the block size 1 k. All spectra and images in these studies were cardiac gated and acquired with an effective repetition time (TR) of 428 ms (two cardiac cycles at 280 beats per minute). The time domain data were multiplied by an exponential line-broadening function of 20 Hz before Fourier transformation and phasing.

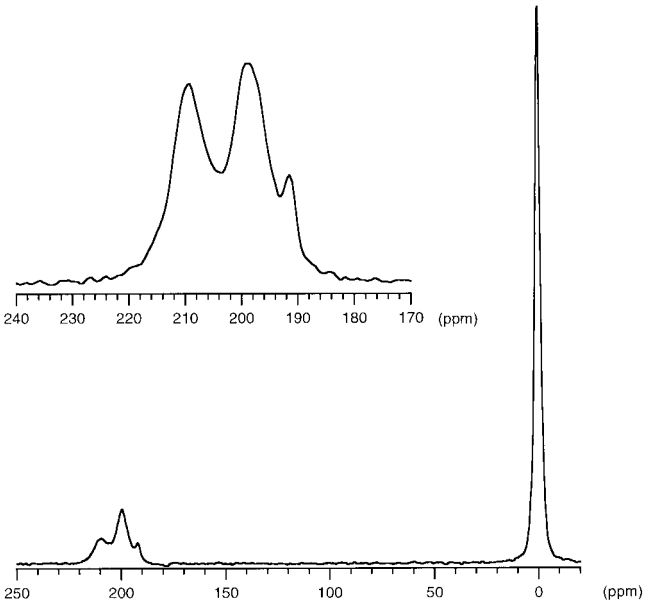

FIG. 1. In vivo NMR spectra of ^{129}Xe in the rat body. The full spectrum shows ^{129}Xe dissolved in blood, tissue, and fat at 210, 199 and 192 ppm, respectively. Xenon gas in lungs is set to 0 ppm. The tip angle used to acquire the full spectrum was 13°, allowing magnetization to build up in tissue and causing the tissue resonance to be larger than the blood resonance. The inset shows a spectrum of the blood/tissue resonances acquired from another experiment with a tip angle of 30°. The tissue component is relatively smaller in the inset spectrum and the blood resonance correspondingly larger because the magnetization is sampled (and destroyed) in the blood before perfusing to distant organs.

The spectrum shown in the inset of Fig. 1 was acquired with similar parameters. To minimize destruction of xenon magnetization in the gas phase, a 200-μs radiofrequency (RF) pulse was used, and the frequency of the spectrometer was shifted so that the peaks around 200 ppm were on resonance. This procedure places the gas resonance near the null point in the frequency excitation profile of the RF pulse. The tip angle was measured to be 30° for the blood/tissue resonances and estimated to be approximately 1° for the gas resonance. The spectrum in the Fig. 1 inset was acquired from a single experiment of about 25 seconds' breathing of the xenon/oxygen mixture.

One-Dimensional CSI

One-dimensional chemical-shift images were collected along the anterior-posterior axis of the animal. Localized ^{129}Xe spectra from 220 to 180 ppm are shown in Fig. 2 and reveal xenon dissolved in blood, tissue, and fat. Two experiments were performed: one with a 30° tip angle and

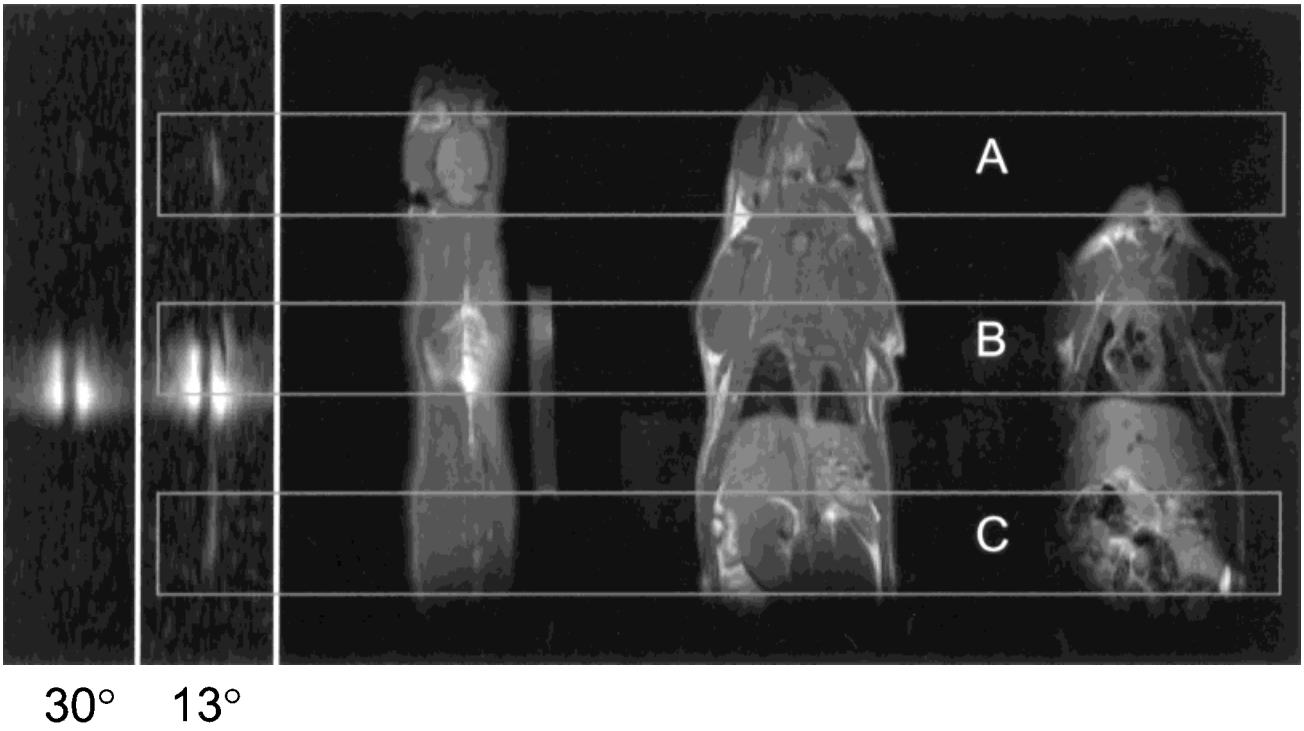

FIG. 2. One-dimensional CSI of ^{129}Xe dissolved in blood, tissue, and fat in the rat body and ^{1}H spin-echo images for anatomical registration. CSI data of the blood and tissue resonances (from 220 to 180 ppm) are presented as grayscale images. Results of two experiments at 30° and 13° tip angle are presented. With a 13° tip angle, sufficient magnetization accumulates in the brain and kidney. With a tip angle of 30°, ^{129}Xe magnetization is sampled and destroyed in the thorax before it has a chance to reach the brain or kidney. The resonance at 192 ppm is present only near the heart and hence is assigned to xenon dissolved in epicardial fat. The boxes labeled A, B, and C correspond to the regions used to construct the localized spectra in Fig. 3.

the other with a 13° tip angle as indicated in Fig. 2. The field-of-view (FOV) for each experiment was 180 mm with 64 phase-encoding steps. The duration of the phase-encode gradient was 500 μs. All other parameters are as in the Fig. 1 inset. No slice selection was used in these one-dimensional (1D) CSI experiments. Xenon delivery commenced about 5 seconds before the start of the pulse sequence and continued throughout the 1-minute acquisition.

The data were processed with 20-Hz line broadening in the time domain and a trapezoidal function in k space. The k_z dimension was zerofilled from 64 to 128 data points. The data were Fourier transformed in both dimensions and are presented as a grayscale image in phase-sensitive mode in Fig. 2. A series of spin-echo proton images with 2-mm slice thickness (TR 428 ms, TE 18 ms, FOV 180 mm) was recorded for anatomical registration of the localized ^{129}Xe spectra. Slices of proton images containing brain, kidney, and heart are shown in Fig. 2.

The regions labeled A, B, and C on Fig. 2 in the 13° 1D CSI experiment were summed over the spatial regions as indicated by the boxes. The spectra corresponding to the boxed regions are shown in Fig. 3 a, b, and c.

Two-Dimensional CSI

Axial and coronal images of xenon in blood, tissue, and gas are shown in Figs. 4 and 5. Figure 4 shows the grayscale xenon and proton images, and Fig. 5 shows a false color rendition of the xenon images superimposed on the proton images for anatomical registration. Xenon was delivered to the animal for approximately 4 minutes, during which time data were acquired. Each dataset was acquired with 16×16 phase-encoded values and two averages per phase-encode line. The FOV was 60×60 mm in the axial images (Fig. 4 A–D and Fig. 5 A–C) and 100×100 mm in the coronal images (Fig. 4 E–H and Fig. 5 D–F). The axial xenon images were created from a single dataset with a 4-minute signal acquisition, and the coronal images were created from the sum of two 4-minute acquisitions. No slice selection was used. With a 30° tip angle and a 428-ms TR, xenon magnetization is sampled and destroyed in the thorax before it can perfuse to the brain or kidney (see the 1D CSI data shown in Fig. 2). Other parameters are as in the Fig. 1 inset.

Each dataset was multiplied by a 20-Hz line broadening function in the time domain and a trapezoidal function in both k_x and k_z or k_x and k_y. k-Space was zerofilled from 16×16 to 32×32. The data were then Fourier transformed along each dimension and the magnitude was calculated. Summing the two-dimensional (2D) planes across each resonance (blood, tissue, and gas) created images shown in Figs. 4 and 5. Cardiac-gated proton images, with an appropriate FOV, were collected for spatial registration of the ^{129}Xe signal. Water from the warming blanket is seen on the top in Fig. 4D and Fig. 5 A–C.

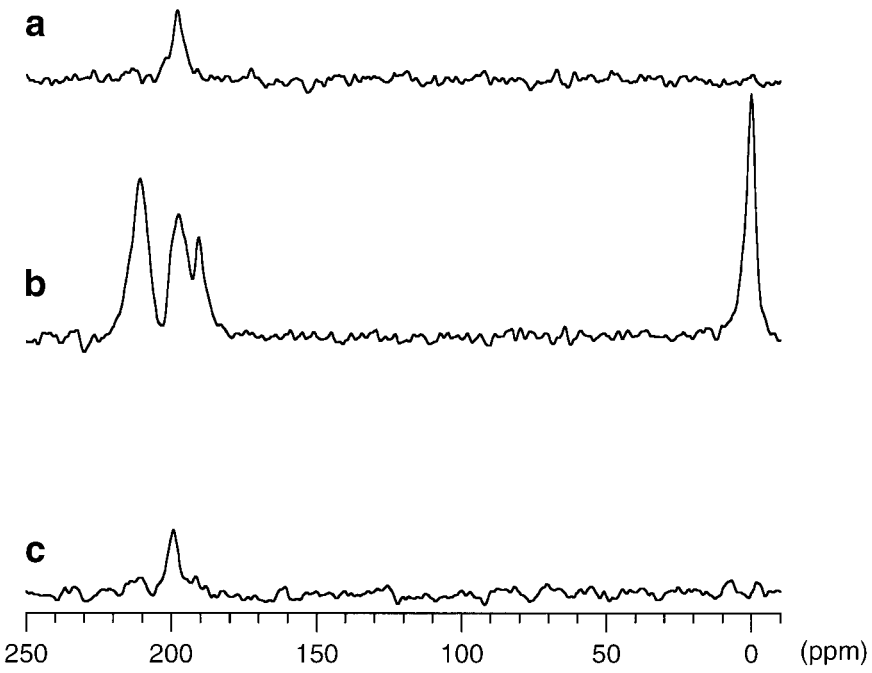

FIG. 3. Localized spectra of ^{129}Xe in the rat body. Spectra of ^{129}Xe from regions encompassing the brain (**a**), heart (**b**), and kidney (**c**). Each spectrum was obtained by summing the 1D CSI data over the respective regions indicated on Fig. 2. The tip angle in this study was 13°.

Two representative ^{129}Xe spectra from the axial 2D CSI dataset, displayed on the same vertical scale, are shown in Fig. 6. Figure 6a shows the spectrum of a voxel located near the heart ventricle, and Fig. 6b shows the spectrum of a voxel located in the lungs.

Dynamics

Uptake and washout of each resonance of ^{129}Xe in the rat body are shown in Fig. 7. A series of 64 spectra was recorded with two phase-cycled averages each. The frequency and line width of each resonance was determined by fitting a multiple Lorentzian model to the spectrum in the Fig. 1 inset. With these parameters fixed, the amplitude of each peak for each of the 64 spectra was determined by χ^2 minimization. This procedure assumes that the frequency and width of each resonance is constant throughout the uptake and washout. The results are shown in Fig. 7 for xenon in gas, fat, tissue, and blood. The amplitude of the xenon gas resonance was normalized to the amplitude

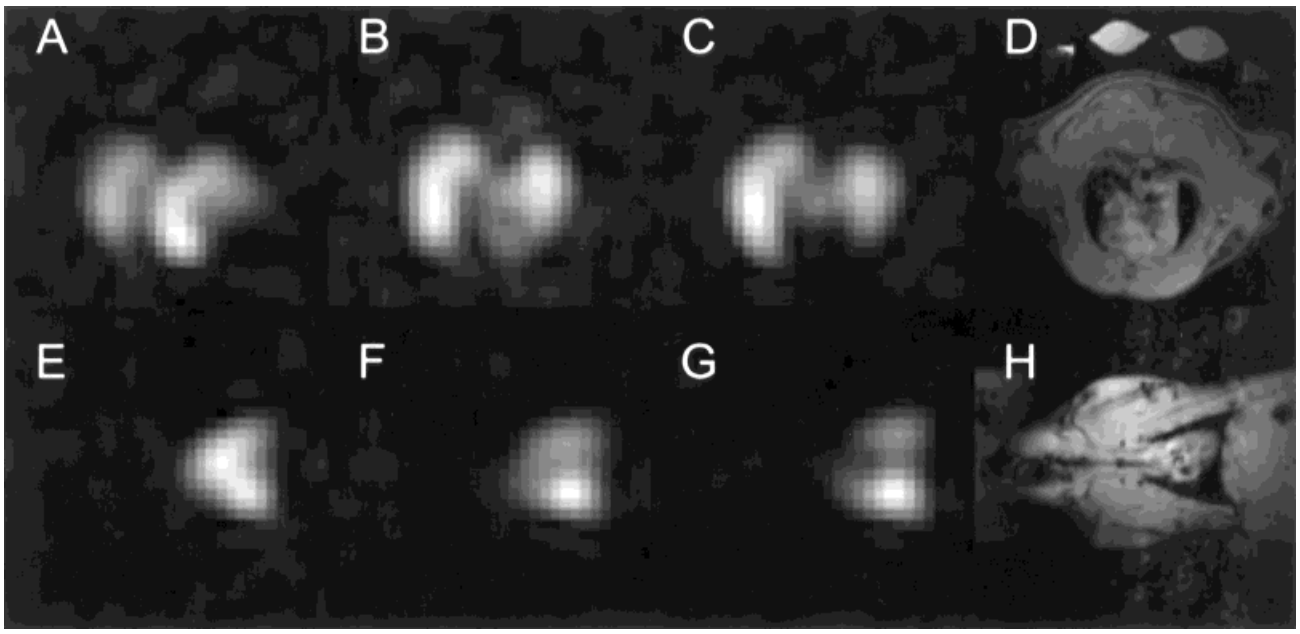

FIG. 4. ^{129}Xe axial (**A–C**) and coronal (**E–G**) 2D CSI. Images of ^{129}Xe in blood (**A** and **E**), tissue (**B** and **F**), and gas (**C** and **G**) are presented. Cardiac-gated proton images (**D** and **H**) are shown for anatomical registration. The FOV was 60 × 60 mm in the axial images (**A–D**) and 100 × 100 mm in the coronal images (**E–H**). The tip angle was 30° for all images.

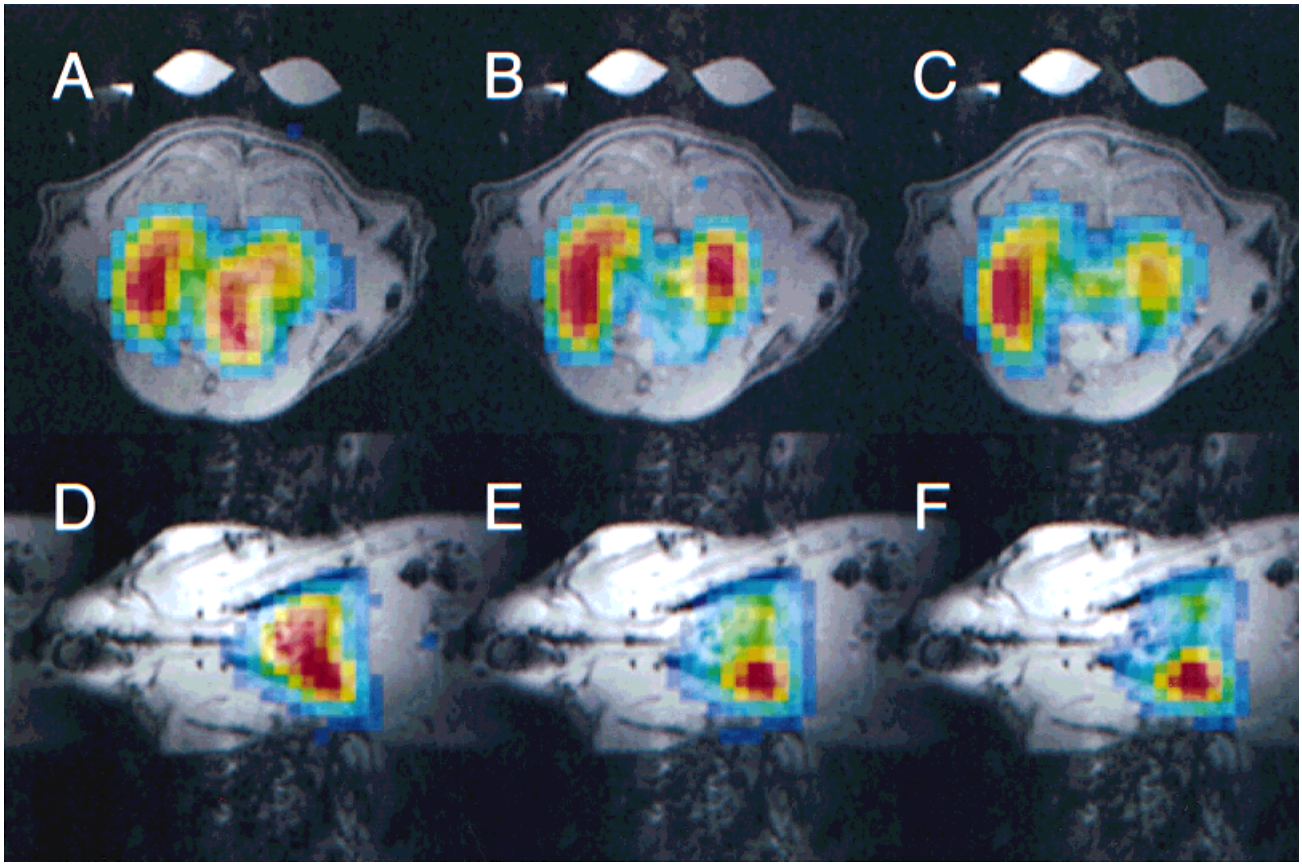

FIG. 5. Color overlay of the axial (**A–C**) and coronal (**D–F**) ^{129}Xe images onto the ^{1}H images. Images of ^{129}Xe dissolved in blood (**A** and **D**) show xenon in lung vasculature and in the heart ventricle. Images of ^{129}Xe dissolved in tissue (**B** and **E**) show xenon dissolved in the lung parenchyma and in the myocardium. A difference between the gas images (**C** and **F**) and the blood images (**A** and **D**) can be used to assess lung function in a single MRI study. Images of ^{129}Xe dissolved in the myocardium can be used to create a map of myocardial perfusion.

of the resonance of xenon dissolved in blood in Fig. 7a. The magnetization of xenon dissolved in blood, tissue, and fat are shown on the same scale in Fig. 7b. Delivery of the xenon/oxygen mixture started at approximately $t = 5$ seconds, and continued to $t = 30$ seconds (Fig. 7). The tip angle in this study was 30°. Figure 8 shows three spectra obtained at the beginning (a), middle (b), and end (c) of xenon delivery to the animal. Each spectrum was acquired in 4 seconds. The tip angle used to acquire the spectra in Fig. 8 was 13°.

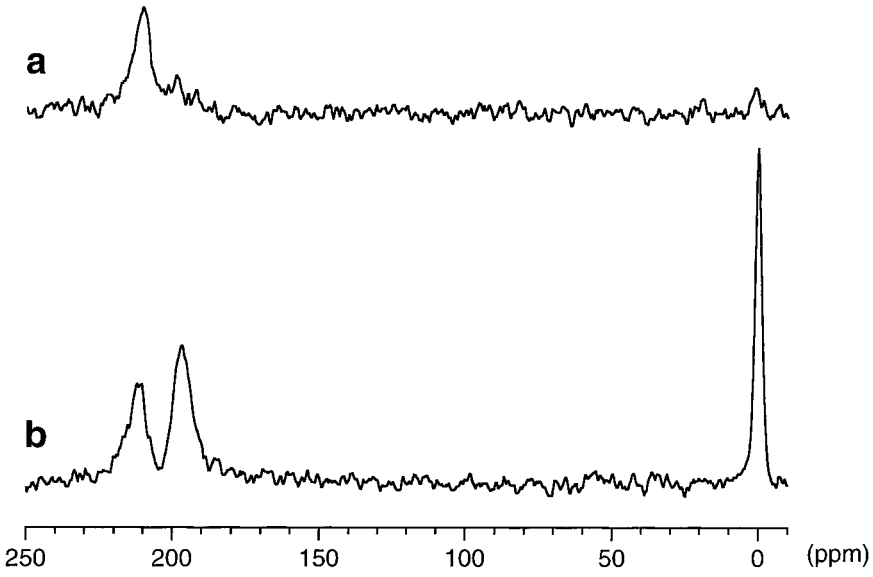

FIG. 6. Spectra of ^{129}Xe constructed from a single voxel of the 2D CSI data located in the heart ventricle (**a**) and lungs (**b**) in Sprague-Dawley rats. Each spectrum was extracted from the data shown in Figs. 4 and 5. The single resonance observed in blood in the heart ventricle at 210 ppm (**a**) is consistent with fast exchange of xenon between red blood cells and plasma.

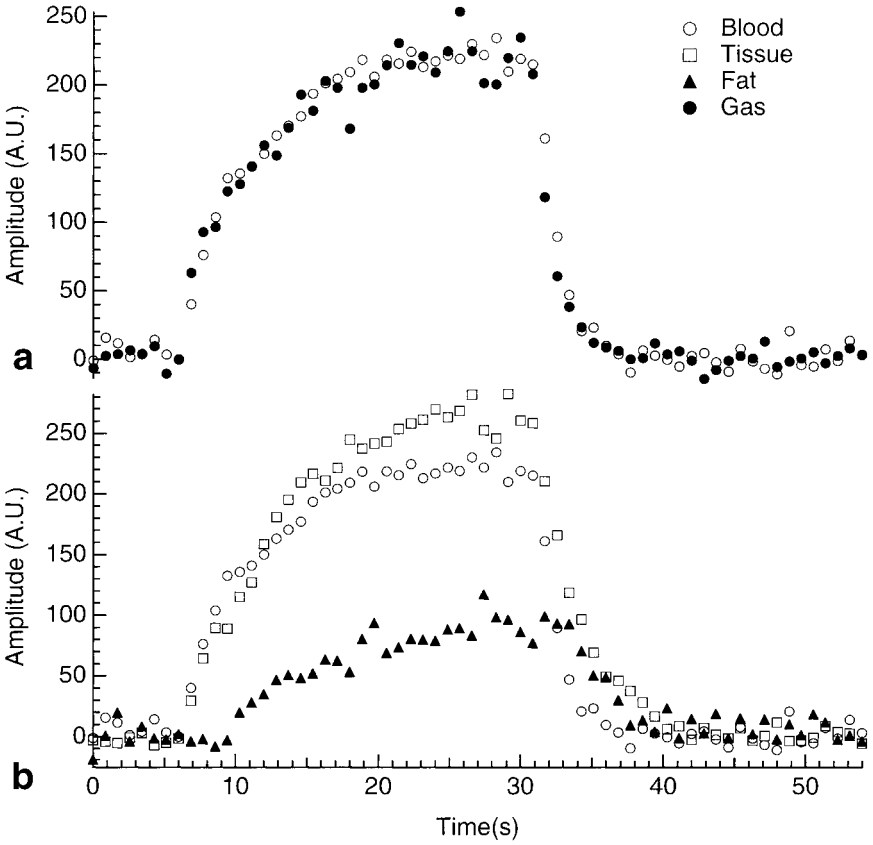

FIG. 7. Dynamics of ^{129}Xe magnetization in vivo. **a:** The uptake and washout of xenon gas (●) and xenon dissolved in blood (○). The dynamics of the blood resonance match the dynamics of the gas resonance and demonstrate efficient exchange of xenon between gas and blood in the lung. **b:** Dynamics of xenon dissolved in blood (○), tissue (□), and fat (▲). The tip angle in this experiment was 30° and the TR was 428 ms.

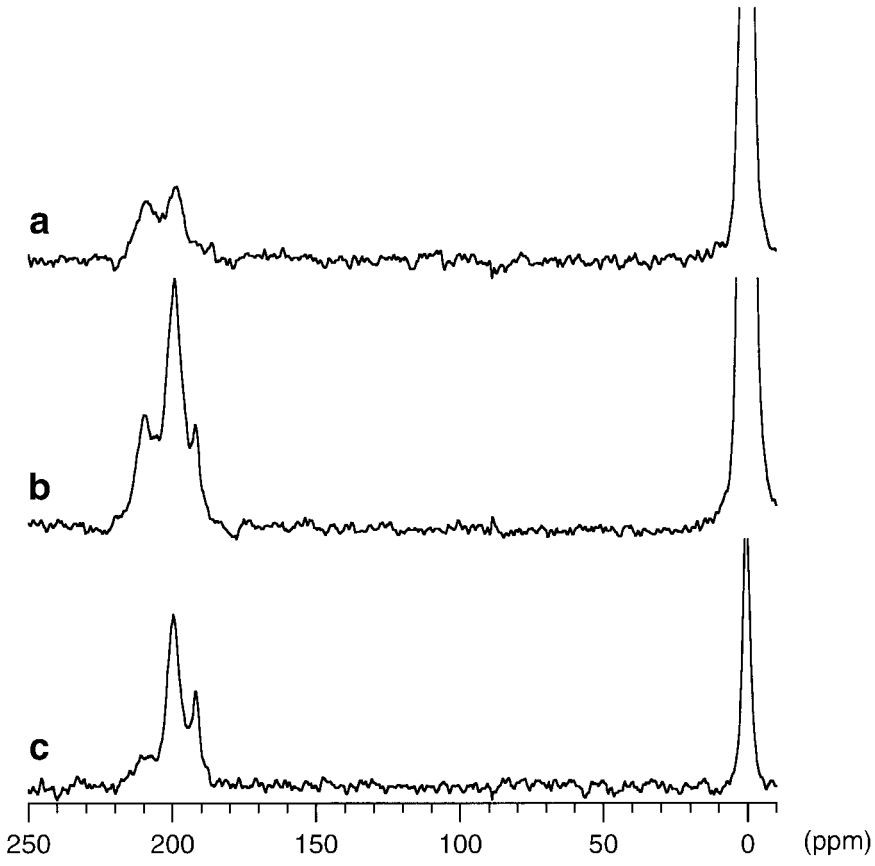

FIG. 8. Spectra obtained at the beginning (**a**), middle of (**b**), and end of (**c**) xenon gas delivery. All spectra are plotted on the same vertical scale and were acquired over a period of four seconds. **a:** Xenon in gas, tissue, and blood is present at the onset of the delivery of xenon gas. The resonance of xenon dissolved in tissue is probably caused by xenon in lung epithelium at this early time in the uptake. The resonance of xenon in fat is absent. **b:** All three resonances are near equilibrium, with the tissue resonance clearly larger than either the blood or the fat resonance. **c:** At the end of xenon delivery, the coupled blood and gas peaks are small. The resonances of xenon dissolved in tissue and in fat remain. The resonance at 192 ppm, assigned to xenon dissolved in fat, does not appear at the onset of xenon delivery in **a** and remains after the blood component has nearly disappeared in **c**. The tip angle in this experiment was 13°.

RESULTS AND DISCUSSION

Spectroscopy

The spectra of ^{129}Xe in the rat body shown in Fig. 1 were acquired with tip angles of 13° (full spectrum) and 30° (inset spectrum). The data presented here are consistent with xenon dissolved in blood (210 ppm), xenon dissolved in tissue (199 ppm), xenon dissolved in fat (192 ppm), and xenon gas (0 ppm). As described above, each spectrum in Fig. 1 represents an average, steady-state spectrum acquired with repeated RF pulsing. The relative amplitudes of xenon magnetization in blood, tissue, and gas are different in the main spectrum and the inset in Fig. 1. The difference arises because the larger tip angle used to acquire the spectrum in the inset destroys xenon magnetization in the blood before it has a chance to perfuse to distant organs such as brain and kidney. The effective transverse relaxation time, T_2^*, was determined by the width of a Lorentzian fit to each resonance and found to be approximately 2 ms for ^{129}Xe dissolved in blood or tissue, 7 ms for ^{129}Xe dissolved in fat, and 5 ms for ^{129}Xe gas in the lungs.

One-Dimensional CSI

The magnetization of laser-polarized ^{129}Xe was localized in the rat body with 1D CSI (Fig. 2). Spectrally resolved images were acquired along the anterior-posterior axis of the animal to obtain the spatial distribution of xenon magnetization dissolved in blood, tissue, and fat. One-dimensional CSI images show that ^{129}Xe magnetization in blood is present in the thorax (lungs and heart) and that ^{129}Xe magnetization in tissue is present in the brain and abdomen (kidney and/or liver) in addition to the thorax. The effect of tip angle on the spatial distribution of xenon magnetization is shown in Fig. 2. With a 13° tip angle, ^{129}Xe magnetization is observed in all perfused tissues. This occurs because the rate of destruction of ^{129}Xe magnetization is slow compared with the rate of transfer to the tissue. With a 30° tip angle, ^{129}Xe magnetization is observed only in the thorax; longitudinal magnetization is sampled and destroyed in the thorax before it can reach the more distant organs, such as the brain or the kidneys.

It is apparent that the resonance at 192 ppm is localized to a region near the heart (Fig. 2) and therefore could be caused by xenon dissolved in myocardial tissue or xenon dissolved in fat. The data in Fig. 2 indicate that the intensity of the signal decreases when the tip angle is increased from 13° to 30°. Combined with the time-resolved spectroscopic studies presented below, this is consistent with slowly perfused adipose tissue. In addition, this resonance only appears near the heart and is probably caused by xenon dissolved in epicardial fat.

Localized ^{129}Xe spectra, created by summing over the boxed regions shown in Fig. 2, are presented in Fig. 3. Figure 3a corresponds to the boxed region of the brain indicated in Fig. 2. Similarly, Fig. 3b corresponds to the region of the thorax, and Fig. 3c corresponds to the region of the kidneys. Figure 3a shows a single resolved peak in the brain, consistent with our previous findings in the rat brain (10,11) and with other findings in the human brain (12). Figure 3b shows the xenon spectrum in the region of the heart. Xenon dissolved in blood, tissue, and epicardial fat is clearly present. Figure 3c shows a spectrum from the abdominal region of the rat. Although this resonance could arise from xenon in liver, fat, or kidney, it is most likely from xenon in kidney. This conclusion is, based on the high kidney perfusion rate, the chemical shift of the resonance, and the spatial location of the resonance.

Two-Dimensional CSI

One-dimensional CSI experiments demonstrate that ^{129}Xe magnetization is present in the brain, kidney, and thorax of Sprague-Dawley rats after inhalation of laser-polarized ^{129}Xe gas. The 1D CSI data, together with the known biological properties of xenon, show that it will be possible to create quantitative maps of tissue perfusion in the brain and kidney. To provide a clearer picture of the distribution of xenon magnetization in the thorax, a series of 2D CSI experiments was performed. In Figs. 4 and 5 we show the spatial distribution of xenon magnetization in the blood, tissue, and gas components in the thorax. Both axial and coronal projection images were acquired. The xenon signal was localized to the thorax by sampling the magnetization with a 30° tip angle, as discussed above.

The images of ^{129}Xe dissolved in blood (Figs. 4A, 4E, 5A, and 5D) show xenon present in the lung capillary bed, the pulmonary veins, and the left ventricle of the heart. A strong blood signal is found throughout the lungs, indicating efficient transport of xenon from gas in the lungs to blood in the lungs. These images of xenon in blood in the lungs represent the first use of laser-polarized ^{129}Xe to measure transport of xenon gas across the lung epithelium and into blood. Because blood is most concentrated in the heart, the greatest signal intensity in the image of the blood resonance arises from the xenon in blood in the left ventricle of the heart.

The images of ^{129}Xe gas (Figs. 4C, 4G, 5C, and 5F) show xenon present in the air space of the lungs and trachea. Although images constructed from CSI data may have lower resolution than the high-resolution in vivo images of ^{3}He gas (18), high spatial resolution is often not needed for critical clinical decisions in pulmonary medicine. What is needed is a measure of lung function. A difference between the distribution of xenon in blood and gas in the lung would show a defect, such as a pulmonary embolism. This is an example of how ^{129}Xe MRI could be used to assess lung function. Thus, ^{129}Xe CSI and other frequency-selective imaging methods have the potential to replace standard ventilation-perfusion techniques with a single MRI study.

The images of xenon dissolved in tissue in the thorax (Figs. 4B, 4F, 5B, and 5E) arise predominately from xenon dissolved in the lung epithelium. This finding is consistent with the spectroscopic and dynamic results presented below that show xenon passing through a tissue phase in the lungs before reaching the pulmonary blood. Xenon magnetization in tissue is also observed in the region of the heart (Figs. 4B and 5B) and indicates that xenon is present in myocardial tissue. The presence of xenon magnetization in the myocardium allows MRI of laser-polarized ^{129}Xe to be used to measure cardiac perfusion, similar to the manner in which ^{133}Xe signals are used in nuclear medicine (4). The blood and tissue resonances in the lung are broadened by magnetic field inhomogeneities caused by

the air-tissue interface and may account for the relatively broad tissue phase signals observed in the thorax. Since the gyromagnetic ratio of ^{129}Xe is about four times less than the gyromagnetic ratio of ^{1}H, susceptibility broadening is less severe for ^{129}Xe than for ^{1}H.

Figure 6a shows the spectrum of a single voxel of the axial 2D CSI dataset located near the left ventricle in the heart. This volume consists primarily of blood. The most prominent feature in Fig. 6a is the large, single resonance observed at 210 ppm. Previous in vitro spectroscopic studies show two resonances in human blood identified as red blood cells and blood plasma (13,14). Figure 6b is the spectrum from a voxel located in the lungs and shows xenon in the gas, blood, and tissue of the lungs. The gas resonance is relatively small because the gas magnetization is tipped only 1° by the 200 μs RF pulse, whereas the blood and tissue components are tipped approximately 30°. The ability to monitor xenon magnetization in the gas, in the tissue, and in the blood in the lungs may provide measures of lung function more sensitive than those currently available with nuclear medicine techniques.

Dynamics

The dynamics of xenon magnetization in gas, blood, tissue, and fat are presented in Figs. 7 and 8. Figure 7a shows that xenon magnetization in blood is proportional to xenon magnetization in gas, demonstrating exchange between the gas and blood components in the lungs that is fast on the time scale of 500 ms.

The uptake and washout of xenon magnetization dissolved in blood, tissue, and fat are shown in Fig. 7b. The amplitude of the blood resonance plateaued after about 13 seconds of xenon delivery, but the amplitudes of the tissue and fat resonances continued to grow and had not yet leveled off when xenon delivery was stopped at about 25 seconds. Organs such as the brain, the kidneys, the liver, and the heart have more capacity for xenon because of their blood-tissue partition coefficients and their greater partial volume compared with blood. The apparent uptake and washout rates of ^{129}Xe in fat are slightly slower than the uptake and washout rates for ^{129}Xe in tissue (Fig. 7), consistent with a slower perfusion rate in fat.

The spectra shown in Fig. 8, obtained at the beginning, middle, and end of xenon delivery, help clarify the assignments of the blood and tissue resonances. At the beginning of xenon delivery (Fig. 8a), xenon is present in blood and tissue with the tissue resonance larger than the blood resonance. Because the tissue resonance appears soon after the start of xenon delivery, it most likely arises from xenon in lung parenchyma. Similarly, the blood resonance in Fig. 8a must be from xenon in the lung capillary bed. Figure 8b shows the xenon spectrum just before the time when xenon delivery has stopped. All three resonances are present, and the tissue resonance is much larger than either the fat or the blood resonance. After delivery of xenon gas has stopped, the gas and blood resonances have nearly disappeared (Fig. 8c), whereas the tissue and fat resonances remain.

Assignments

The data presented here are consistent with xenon dissolved in blood (210 ppm), tissue (199 ppm), and fat (192 ppm). These assignments are indicated by the spatial distribution of xenon (Figs. 2–5), the in vivo spectrum obtained from the heart ventricle (Fig. 6a), and the dynamics of xenon in vivo (Figs. 7 and 8).

Previous in vitro work has shown that ^{129}Xe magnetization in human blood has resonances at 216 and 192 ppm assigned to xenon in red blood cells and xenon in plasma, respectively (13,14). Studies at 9.4 T and ambient laboratory temperature found that the magnetization of these resonances is coupled by exchange of xenon between the two components (14). Because of exchange, one would expect that spectra of ^{129}Xe dissolved in blood would always have two resonances in vivo. These findings have led others (9) to assign the resonances of nonlocalized, in vivo, ^{129}Xe spectra to xenon in red blood cells (213 ppm), xenon in tissue (199 ppm), and xenon in fat or plasma (191 ppm). We find no evidence for two blood resonances in Sprague-Dawley rats in vivo. The spectrum of ^{129}Xe localized to the left ventricle of the heart, where the highest concentration of blood in the thorax is present, consists of one dominant resonance at 210 ppm (Fig. 6a). Figure 8a shows a resonance at 210 ppm at the onset of xenon delivery. This resonance could be assigned to xenon in red blood cells, but no corresponding plasma resonance is present at 192 ppm. In Fig. 8c, a resonance is present at 192 ppm but no resonance is observed at 210 ppm. Our data require a different assignment of the resonances, as indicated above.

A variety of factors could contribute to the observation of one resonance in rat blood in vivo. Hemoglobin of Sprague-Dawley rats may have a different affinity for xenon than human hemoglobin and may create a different chemical shift. The rat red blood cell is known to be smaller than the human red blood cell (19), allowing more efficient mixing of the two components. In the fast exchange limit, the frequency of the blood resonance, ν_{blood}, is given by a weighted average of the frequencies of the red blood cell (rbc) component, ν_{rbc}, and the plasma component, ν_{plasma}:

$$\nu_{blood} = p_{rbc}\nu_{rbc} + p_{plasma}\nu_{plasma}. \quad [1]$$

The coefficients p_{rbc} and p_{plasma}, the mole fractions of xenon in red blood cells and plasma, are determined by the red blood cell-plasma partition coefficient for xenon, λ_{cp}, and the hematocrit, H_{ct}:

$$p_{rbc} = \frac{1}{1 + \frac{1 - H_{ct}}{H_{ct}\lambda_{cp}}} \text{ and } p_{plasma} = \frac{1}{1 + \frac{H_{ct}\lambda_{cp}}{1 - H_{ct}}}. \quad [2]$$

Using previously measured values, it is possible to estimate the blood resonance frequency under fast exchange conditions. We set ν_{rbc} to 216 ppm and ν_{plasma} to 199 ppm (as previously reported (13,14)), the hematocrit to 42%, and λ_{cp} to 2.55. (The xenon partition coefficient is 2.27 ± 0.07 in human blood and 3.31 ± 0.06 in dog blood (20)). With these parameters, Eqs. [1] and [2] yield a value of 210 ppm for ν_{blood}, the same chemical shift as measured

in vivo. This analysis shows that our observations are consistent with ^{129}Xe in fast exchange between the red blood cell and plasma components. The data and the analysis presented here do not explain, at a fundamental level, the discrepancies observed between xenon in human blood in vitro and xenon in rat blood in vivo. More work is needed to fully understand the differences observed in ^{129}Xe magnetization in different species and under different experimental conditions.

The resonance at approximately 199 ppm first appears in lung parenchyma after xenon gas is introduced into the lungs (Fig. 8a). The tissue signal grows with time and becomes larger than the signal of ^{129}Xe dissolved in blood as xenon perfuses into more distant organs such as brain and kidney (Figs. 1 and 8b). One-dimensional CSI data acquired with a low–tip-angle pulse show that xenon magnetization at 199 ppm is present in the thorax, the kidneys, and the brain (Fig. 2). Two-dimensional CSI data show xenon magnetization at this frequency in the thorax, in the lungs and in the heart (Figs. 4B and 5B). Our previous work (10) has shown that the spectrum of ^{129}Xe in the brain is dominated by a single resonance: xenon dissolved in brain tissue. The resonance at 199 ppm is consistent with ^{129}Xe magnetization dissolved in tissue.

The resonance observed at 192 ppm is assigned to xenon in epicardial fat based on chemical shift, dynamics, and location in the rat body, as discussed above. The chemical shift of this resonance is similar to the chemical shift of xenon dissolved in beef fat (9) or long-chain fatty acids (21). Autoradiography has shown that ^{133}Xe accumulates in epicardial fat at steady-state (22). Because nuclear medicine does not differentiate between ^{133}Xe in myocardial tissue and ^{133}Xe in epicardial fat, ^{133}Xe is currently not a preferred method for measuring cardiac perfusion (4,23). We have shown that ^{129}Xe magnetization in epicardial fat and in myocardial tissue are easily separated with NMR methods.

CONCLUSION

The results presented here show that ^{129}Xe magnetization is present in lungs, blood, brain, kidney, myocardium, and epicardial fat after inhalation of laser-polarized ^{129}Xe. ^{129}Xe resonances are observed in vivo at 210, 199, and 192 ppm and are consistent with ^{129}Xe magnetization dissolved in blood, tissue, and epicardial fat, respectively. ^{129}Xe magnetization flows from gas in lungs, to lung epithelium, into the blood, through the heart, and finally into organs (heart, brain, and kidney). In the heart ventricle, a single blood resonance is observed, indicating that the red blood cell and plasma components are in fast exchange in vivo at 37°C and 2T in rat blood. A difference between the distribution of ^{129}Xe gas in the lungs and in blood in the lungs allows assessment of lung function in a single MRI study. In a separate paper, we show that ^{129}Xe MRI with appropriate RF sampling can be used to measure tissue perfusion. Increases in ^{129}Xe polarization from the current 5% to 8% to realistic levels of 35% will allow spatial resolution comparable to that of standard proton MR images.

ACKNOWLEDGMENTS

The authors thank Phillip Sherman for animal preparation and Jon Zerger and Nathan Stokes for the multiple Lorentzian fitting routine.

REFERENCES

1. Chen RYZ, Fan FC, Kim S, Jan KM, Usami S, Chien S. Tissue-blood partition coefficients of xenon: temperature and hematocrit dependence. J Appl Physiol 1980;49:178–181.
2. Kety SS. The theory and application of the exchange of inert gas at the lung tissue. Pharmacol Rev 1951;3:1–41.
3. Cosgrove MD, Mowat P. Evaluation of the xenon-133 renal blood flow method. Br J Urol 1974;46:134–147.
4. Marcus ML, Wilson RF, White CW. Methods of measurement of myocardial blood flow in patients: a critical review. Circulation 1987;76: 245–253.
5. Lassen NA. Cerebral blood flow tomography with xenon-133. Semin Nucl Med 1985;15:347–356.
6. Alderson PO. The role of Xe-133 ventilation studies in the scintigraphic detection of pulmonary embolism. Radiology 1976;120:633–650.
7. Andersen AM, Ladefoged J. Partition coefficient of ^{133}Xe between various tissues and blood in vivo. Scand J Clin Lab Invest 1967;19:72–78.
8. Wagshul ME, Button TM, Li HF, Liang Z, Springer CS, Zhong K, Wishnia A. In vivo MR imaging and spectroscopy using hyperpolarized ^{129}Xe. Magn Reson Med 1996;36:183–191.
9. Sakai K, Bilek AM, Oteiza E, Walsworth RL, Balamore D, Jolesz FA, Albert MS. Temporal dynamics of hyperpolarized ^{129}Xe resonances in living rats. J Magn Reson Series B 1996;111:300–304.
10. Swanson SD, Rosen MS, Agranoff BW, Coulter KP, Welsh RC, Chupp TE. Brain MRI with laser-polarized ^{129}Xe. Magn Reson Med 1997;38:695–698.
11. Rosen MS, Chupp TE, Swanson SD, Coulter KP, Welsh RC. Polarized ^{129}Xe optical pumping/spin exchange and delivery system for magnetic resonance spectroscopy and imaging studies. Rev Sci Instr 1999;70: 1546–1552.
12. Mugler JP, Driehuys B, Brookeman JR, Cates GD, Berr SS, Bryant RG, Daniel TM, deLange EE, Downs JH, Erickson CJ, Happer W, Hinton DP, Kassel NF, Maier T, Phillips CD, Saam BT, Sauer KL, Wagshul ME. MR imaging and spectroscopy using hyperpolarized Xe-129 gas: preliminary human results. Magn Reson Med 1997;37:809–815.
13. Albert M, Schepkin VD, Budinger TF. Measurement of ^{129}Xe T_1 in blood to explore the feasibility of hyperpolarized ^{129}Xe MRI. J Comput Assist Tomogr 1995;19:975–978.
14. Bifone A, Song YQ, Seydoux R, Taylor RE, Goodson BM, Pietrass T, Budinger TF, Navon G, Pines A. NMR of laser-polarized xenon in human blood. Proc Natl Acad Sci USA 1996;93:12932–12936.
15. Wilson GJ, Santyr GE, Anderson ME, DeLuca PM. Longitudinal relaxation times of ^{129}Xe in rat tissue homogenates at 9.4 T. Magn Reson Med 1999;41:933–938.
16. Jameson CJ, Jameson AK, Hwang JK. Nuclear-spin relaxation by intermolecular magnetic dipole coupling in the gas phase—Xe-129 in oxygen. J Chem Phys 1988;89:4074–4081.
17. Alderman DW, Grant DE. An efficient decoupler coil design which reduces heating in conductive samples in superconducting spectrometers. J Magn Reson 1979;36:447–451.
18. MacFall JR, Charles HC, Black RD, Middleton H, Swartz JC, Saam B, Driehuys B, Erickson C, Happer W, Cates GD, Johnson GA, Ravin CE. Human lung air spaces: potential for MR imaging with hyperpolarized He-3. Radiology 1996;200:553–558.
19. Farris EJ, Griffith JQ. The rat in laboratory investigation. Philadelphia: JB Lippincott; 1949.
20. Carlin R, Chien S. Partition of xenon and iodoantipyrine among erythrocytes, plasma, and myocardium. Circ Res 1976;40:497–504.
21. Miller KW, Reo NV, Schoot Uiterkamp AJ, Stengle DP, Stengle TR, Williamson KL. Xenon NMR: chemical shifts of a general anesthetic in common solvents, proteins, and membranes. Proc Natl Acad Sci USA 1981;78:4946–4949.
22. Shaw DJ, Pitt A, Friesinger GC. Autoradiographic study of ^{133}Xe disappearance method for measurement of myocardial blood flow. Cardiovasc Res 1971;6:268–276.
23. Maseri A, Pesola A, L'Abbate A, Contini C, Michelassi C, D'Angelo T. Contributions of recirculation and fat diffusion to myocardial washout curves obtained by external counting in man. Circ Res 1974;35:826–835.